

# ANALYTICAL MODEL FOR BLADE-VORTEX INTERACTION NOISE

L. M. B. C. Campos & F. J. P. Lau

Secção de Mecânica Aeroespacial, ISR,

Instituto Superior Técnico, 1049-001 Lisboa Codex, Portugal.

## Abstract

The sound pulse emitted by a vortex interacting with a helicopter airfoil at arbitrary positive or negative angle-of-attack is considered. A simple analytical expression is obtained assuming that the vortex follows a streamline with a given aiming distance from the airfoil center. The plotting of sound pulses shows that they consist of peaks of rarefaction and compression. The graphics are compared with experimental data from the European Program HELINOISE.

## 1 Introduction

The helicopter is an important subject of acoustical study (Cox & Lynn 1972, Leverton 1989; Lowson 1991) because: (i) there are several sources of noise (main and tail rotors, gearbox and transmission, engines) and several propagation paths (airborne and structure-borne); (ii) the operating conditions, either in civil applications involving flight in populated areas, or in military operations in combat zones, put a high emphasis on reduction of the noise signature.

The main contributor to helicopter low-frequency noise is the rotor, and a substantial literature is devoted to the prediction (Lowson & Ollerhead 1968; Hawkins & Lowson 1974, 1976; Unal & Tung 1989) and measurement (Cox & Lynn 1972; Schmitz & Yu 1986; Schultz & Spletstoeser 1987) of rotor noise. The estimation of the latter can be made at three levels of sophistication: (i) as simple scaling laws, e.g. for Mach number (Aravamudan, Lee & Harris 1975; Humbad 1975); (ii) on the basis of the theory of singularities and surfaces in motion (Lowson 1965; Ffowcs-Williams & Hawkins 1968; Campos 1978a; Farassat 1986) to calculate separate the thickness, loading and quadrupole noise components; (iii) using aerodynamic methods to determine the pressure distribution on the rotor and hence the radiated sound, which is affected by the free vortex wake (Dinyavari & Friedmann 1989; Stangl & Wagner 1994; Röttgermann & Wagner 1994).

One of the main noise generation mechanisms is blade-vortex interaction (Howe 1989, 1990; George & Lyrintsis 1988), which appears as a succession of

pulses in the time domain, or spikes in the frequency domain. The calculation of the broadband component of helicopter noise from the spikes has been addressed elsewhere (Campos 1978b, 1983, 1984, 1986; Campos & Macedo 1992), and we are concerned here with the mechanism of generation of the pulses (Howe 1975; Campos 1978c, 1986), by interaction of a vortex with an airfoil, at arbitrary angle-of-attack; the inclusion of the latter is important to account for blade flapping, during rotation. If the blade flap angle is averaged over a revolution, then the angle-of-attack relative to that flap angle, increases when the helicopter is climbing and decreases when it is descending. Thus it is important to consider arbitrary angles-of-attack, including both large positive and negative values, to represent steep climbs and descents, respectively. It is well-known that the noise field of an helicopter is distinct in hover, forward flight, climb and descent, showing that the velocity and angle-of-attack of the incident stream has important acoustic effects. We address this issue starting with the sound pulse due to the interaction of one vortex with an airfoil, and then proceed to consider multiple, successive pulses.

A vortex can radiate sound as a dipole (Lighthill 1952, Powel 1968, Howe 1975, Campos 1978c), represented by Lamb's vector or vortical force, associated with the component of vorticity transverse to the velocity. This force can be projected on the group velocity, i.e. sound speed in direction of propagation plus convection effect by the mean flow (Blokshintsev 1946; Lighthill 1978; Campos 1978a, 1988), to specify a work per unit time, or activity. If the activity is conserved along the path of the vortex, no sound is radiated, e.g. when it is far from any obstacle disturbing the mean flow. When the activity increases or decreases along the path of the vortex, this is compensated by the emission of respectively a compression or rarefaction pulse. Since, in a spherical wave (Rayleigh 1945; Landau & Lifshitz 1953; Morse & Ingard 1958; Goldstein 1963; Whitham 1974; Lighthill 1978; Pierce 1982) the acoustic pressure integrated over time is zero, the compression and rarefaction parts of the pulse may balance. The sound pulse can be modified, if to the direct wave, radiated by the vortex, is added the sound scattered by the airfoil, which is also a dipole effect. The exact form of the acoustic pressure pulse depends on the airfoil shape, not only because the latter can scatter sound, but

also because it perturbs the incident flow, and thus changes the path of the vortex.

These effects can be illustrated for a Joukowski airfoil, where it is assumed that the vortex travels with the flow. Using this approximation it is possible to calculate analytically the shape of the acoustic pulse in time.

## 2 Blade-Vortex Interaction

In this paper four reference frames are considered:

- $OXYZ$  fixed relative to the wind tunnel, with  $OX$  opposite to the mean flow,  $OZ$  in the vertical direction, and hence  $OY$  horizontal and transverse;
- $Oxyz$  ( $Oy \equiv OY$ ) with  $Oxy$  in the plane of the rotor (figure1), so that this plane makes an angle  $\alpha$  with the mean flow (hence  $\alpha$  is also the angle between  $Oz$  and  $OZ$ );
- $O'\xi v \eta$  with origin at an arbitrary point  $O'$  on the blade axis  $Ov$ , and  $Ov \eta$  in the plane of the rotor;
- $O'\xi_r v_r \eta_r$  with a rotation  $\alpha_p$  equal to the blade pitch around the blade axis  $Ov_r \equiv Ov$ .

The complex potential of the incompressible flow around a circular cylinder of radius  $a$ , is given by

$$f(z) = U_\infty z e^{-i\alpha_t} + U_\infty \frac{a^2}{z} e^{i\alpha_t} + \frac{i\Gamma}{2\pi} \text{Ln}(z), \quad (1)$$

where  $z = x + iy$  and  $U_\infty$  is the mean flow velocity and the angle of attack of the airfoil is denoted by  $\alpha_t$ ; the circulation  $\Gamma$  is given by the Kutta Condition:  $\Gamma = 4\pi a U_\infty \sin \alpha_t$ .

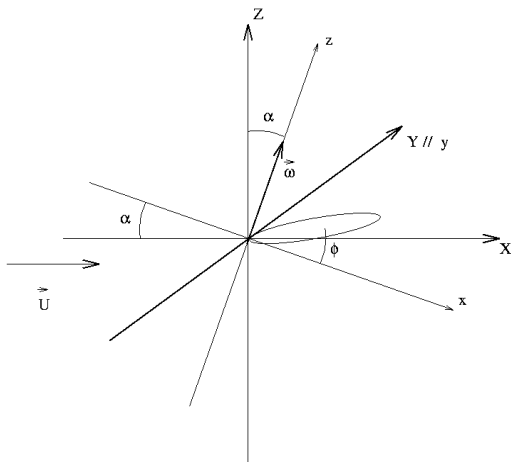


Figure 1: Rotor and Wind tunnel Reference frames.

The complex velocity,

$$\frac{df}{dz} = U_\infty e^{-i\alpha_t} - U_\infty \frac{a^2}{z^2} e^{i\alpha_t} + \frac{2iU_\infty a \sin \alpha_t}{z}, \quad (2)$$

with the Joukowski transformation  $\zeta(z) = z + a/z$ , specifies the complex velocity around a Joukowski airfoil, in the physical plane  $\zeta = \xi + i\eta$ :

$$W(\zeta) = df / d\zeta = (df / dz) / (d\zeta / dz) = \left( \frac{a^2}{a^2 - z^2} \right) U_\infty \left( e^{-i\alpha_t} - \left( \frac{a}{z} \right)^2 e^{i\alpha_t} + i \frac{\Gamma}{2\pi} \right) \quad (3)$$

Using the inverse transformation  $z = \zeta - a^2/\zeta$ , the final expression for the complex velocity is given by:

$$W(r, \theta) = U_\xi - iU_\eta = M_U^{-1} U_\infty \left( r^4 e^{-i4\theta} - 3(ar)^2 e^{-i2\theta} + a^4 \right) \cdot \left\{ \left( r^2 e^{i2\theta} - a^2 \right)^2 e^{-i\alpha_t} - (ar)^2 e^{2i\theta + i\alpha_t} + a \left( \zeta^3 - a^2 \zeta \right) \left( e^{i\alpha_t} - e^{-i\alpha_t} \right) \right\} \quad (4)$$

where

$$M_U \equiv \left| (\zeta^2 - a^2)^2 - a^2 \zeta^2 \right| = r^8 + a^8 - 6(ar)^2 (a^4 + r^4) \cos(2\theta) + 9(ar)^4 + 2(ar)^4 \cos(4\theta) \quad (5)$$

The mean flow velocity is given by

$$\vec{U}_f = U \vec{e}_X = U (\vec{e}_x \cos \alpha_r + \vec{e}_z \sin \alpha_r) \quad (6)$$

in the  $OXYZ$  and  $Oxyz$  reference frame.

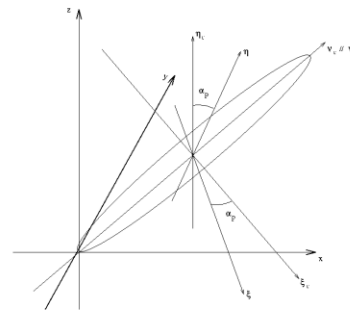


Figure 2: Reference frames  $\zeta$  and  $\zeta_r$ .

The velocity of the origin of both reference frames  $\zeta, \zeta_r$  is given by

$$\vec{U}_0 = -U_0 \vec{e}_{\zeta_r} = U_0 (-\sin(\omega t) \vec{e}_x + \cos(\omega t) \vec{e}_y) \quad (7)$$

where  $U_0 \equiv \omega\sqrt{O_x^2 + O_y^2}$  (figure 3). The mean flow velocity  $\vec{U}_\infty$  measured in this reference frame is equal to  $\vec{U}_\infty = \vec{U}_f - \vec{U}_0$  and its components are:

$$\begin{aligned} U_{\infty,\xi_r} &= U \cos(\alpha) \sin(\omega t) + \omega\sqrt{O_x^2 + O_y^2} \\ U_{\infty,\nu_r} &= U \cos(\alpha) \cos(\omega t) \\ U_{\infty,\eta_r} &= U \sin(\alpha) \end{aligned} \quad (8)$$

The variables  $\alpha_r$  and  $U_\infty$  are given by the projection of  $\vec{U}_\infty$  on the  $\xi_r, \eta_r$  plane (figure 4):

$$\begin{aligned} \tan \alpha_r &= U_{\infty,\eta_r} / U_{\infty,\xi_r} \\ U_\infty &= \sqrt{(U_{\infty,\eta_r})^2 + (U_{\infty,\xi_r})^2} \end{aligned} \quad (9)$$

The velocity used in the complex potential is specified by (9), where  $\alpha_p$  was added to the angle:

$$\vec{U}_\infty = U_\infty e^{-i\alpha_t}; \quad \alpha_t \equiv \alpha_r + \alpha_p. \quad (10)$$

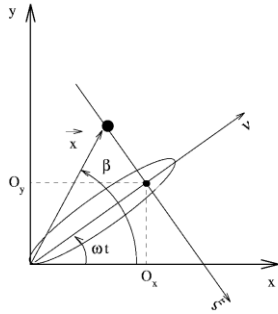


Figure 3:  $Oxyz$  plane of the rotor reference frame and  $O\xi_r\nu_r$  plane of the auxiliary reference frame  $\xi_r$ .

After calculating  $U_\xi$  and  $U_\eta$  (4), it is necessary to obtain them in the reference frame  $Oxyz$  of the rotor, using the transformations:

$$\begin{bmatrix} U_{\xi_r} \\ U_{\eta_r} \end{bmatrix} = \begin{bmatrix} \cos(\alpha_p) & \sin(\alpha_p) \\ -\sin(\alpha_p) & \cos(\alpha_p) \end{bmatrix} \begin{bmatrix} U_\xi \\ U_\eta \end{bmatrix} \quad (11)$$

$$\begin{bmatrix} U_x \\ U_y \\ U_z \end{bmatrix} = \begin{bmatrix} \sin(\omega t) & \cos(\omega t) & 0 \\ -\cos(\omega t) & \sin(\omega t) & 0 \\ 0 & 0 & 1 \end{bmatrix} \begin{bmatrix} U_{\xi_r} \\ U_{\nu_r} \\ U_{\eta_r} \end{bmatrix} + U_0 \begin{bmatrix} -\sin(\omega t) \\ \cos(\omega t) \\ 0 \end{bmatrix} \quad (12)$$

In the last equation, the velocity of the origin of the reference frame was added again.

To simulate the interaction of the blade with a vortex created by another blade, we shall assume that a point vortex is moving with the flow. The Lamb's vector or vortical force is given by:

$$\begin{aligned} \vec{L} &\equiv \rho \vec{\Omega} \times \vec{U} = \\ &= \rho \left\{ \Omega_y U_z \vec{e}_x - \Omega_x U_z \vec{e}_y + (\Omega_x U_y - \Omega_y U_x) \vec{e}_z \right\} \end{aligned} \quad (13)$$

where  $\rho$  is the mass density. The group velocity

$$\vec{W}_g = \vec{U}_f + c\vec{n} \quad (14)$$

is given by the flow velocity, plus the sound velocity on the propagation direction, from the sound source  $(x, y, z)$  to the observer  $(X, Y, Z)$ :

$$\vec{n} \equiv \Delta^{-1} \left\{ (X-x)\vec{e}_x + (Y-y)\vec{e}_y + (Z-z)\vec{e}_z \right\} \quad (15)$$

where  $\Delta \equiv \sqrt{(X-x)^2 + (Y-y)^2 + (Z-z)^2}$ .

The projection of the Lamb's vector (13) on the group velocity (14) specifies the activity

$$\begin{aligned} \vec{A} &\equiv \vec{L} \cdot \vec{W}_g = c\vec{L} \cdot \vec{n} = \rho \Delta^{-1} \left[ \Omega_y U_z (X-x) \right. \\ &\quad \left. - \Omega_x U_z (Y-y) + (\Omega_x U_y - \Omega_y U_x) (X-x) \right] \end{aligned} \quad (16)$$

*i.e.* it represents the work done by the vortex on the group velocity (Lighthill, 1978; Campos, 1992). It can be shown (Howe, 1975; Campos, 1978a, 1986b) that the acoustic pressure is proportional to the material derivative of the activity

$$p(\vec{X}, \vec{x}; t) \equiv \frac{\vartheta}{4\pi c^2 \Delta} \frac{1}{1 + \vec{M} \cdot \vec{n}} \frac{dA}{d\tau} \quad (17)$$

and involves one inverse Doppler factor, where  $\vec{M} = \vec{U}_f / c$  is the Mach number and  $\vartheta$  is the volume occupied by the vortex. In the far field, the following approximation is used:

$$\begin{aligned} 1 + \vec{M} \cdot \vec{n} &= \\ &= 1 + U \left[ (X-x) \cos \alpha + (Z-z) \sin \alpha \right] c^{-1} \Delta^{-1} \end{aligned} \quad (18)$$

The rate-of-change of the activity along the vortex path  $dA/d\tau$  is calculated at the emission time  $\tau$ , which differs from the time of reception  $t$ , by the propagation or retarded time  $t-\tau$ . If the frequency  $\omega$  of sound is specified by the dimensionless Strouhal number  $S_r = \omega l / U$ , where  $l$  is the chord of the airfoil, the ratio of the wavelength of sound to the latter is given by

$$\lambda / d = \frac{2\pi}{kd} = \frac{2\pi c}{f_s d} = \frac{2\pi c}{US_t} = \frac{2\pi}{MS_t}. \quad (19)$$

For a Strouhal number of about unity  $St \sim 1$ , typical of convective emission, and low Mach number mean flow, the wavelength is much larger than the airfoil chord. Thus the airfoil acts as a compact scatterer, *i.e.* the phase differences between reflecting elements are negligible, *viz.* The retarded time is the same for sound originating from all points of the airfoil. It follows that the reception  $t$  and emission time  $\tau$  differ by a constant and thus can be identified within a constant time delay.

The final expression for the acoustic pressure is given by

$$p(\bar{X}, \bar{x}; t) \equiv \frac{dA}{d\tau} \cdot \frac{(\partial/4\pi c)}{c\Delta + U[(X-x)\cos\alpha + (Z-z)\sin\alpha]} \quad (20)$$

where

$$\begin{aligned} \frac{dA}{dt} &= \frac{\partial A}{\partial t} + \bar{U} \frac{\partial A}{\partial \bar{x}} = \\ &= \frac{\partial A}{\partial t} + U_x \frac{\partial A}{\partial x} + U_y \frac{\partial A}{\partial y} + U_z \frac{\partial A}{\partial z} \end{aligned} \quad (21)$$

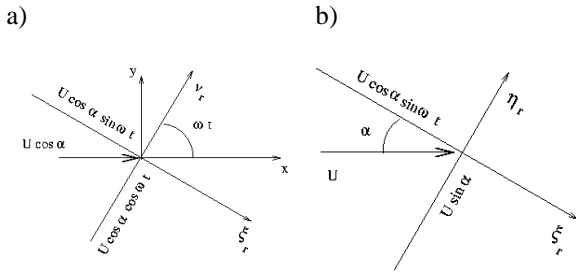


Figure 4: Mean flow velocity  $\bar{U}_f$  projection: a) on the  $O'\xi_r\eta_r$  plane; b) on the  $O'\xi_r\eta_r$  plane

### 3 Vortex Trajectory

During the rotor rotation, the interaction between the incident vortex and each blade is a very complex phenomenon, due to the number of vortices, created by the precedent blades. On a first approximation, it is considered only the interaction between a blade located at an angle  $\phi = \omega t$  and the vortex created by the precedent blade tip (figure 5). The vortex trajectory is given by the equations

$$\begin{aligned} x(T, t) &\equiv r_B \cos[\omega(t-T) + 2\pi/N] + U \cos\alpha T \\ y(T, t) &\equiv r_B \sin[\omega(t-T) + 2\pi/N] \\ z(T, t) &\equiv U \sin\alpha T \end{aligned} \quad (22)$$

where the blade that is creating the vortex is located an angle  $\phi = \omega t + 2\pi/N$ . The blade radius is  $r_B$ , and  $N$  is the number of blades. The variable  $T$  indicates “how long ago” the vortex was created by the blade.

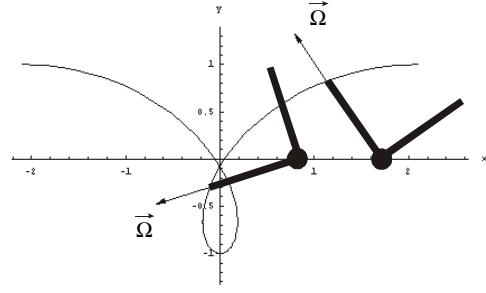


Figure 5: Vortex trajectory

It is assumed that the vorticity is along the blade, when the vortex is created; since the rotor rotation speed is much greater than the mean flow velocity, the vorticity doesn't change its direction along the path and is given by

$$\vec{\Omega}(t, T) \equiv \Omega \left\{ \cos[\omega(t-T) + 2\pi/N] \vec{e}_x + \sin[\omega(t-T) + 2\pi/N] \vec{e}_y \right\} \quad (23)$$

The sound pressure (20) is no longer a function of the vortex coordinates, but rather depends on the variable  $T$ . The sound pressure produced by the vortex-blade interaction is given by the integral of (20) along the vortex trajectory

$$p(\bar{x}; t) = \int_0^{T_f} p(\bar{x}, T, t) dT. \quad (24)$$

In the implementation of the code, the integral was replaced by a sum; the upper limit  $T_f$  corresponds to the intersection point of the vortex trajectory with the next blade at  $\beta = \omega t - 2\pi/N$ .

### 4 Numerical Results

The sound pressure data for a rotor revolution period were compared to the experimental data obtained in the European Program HELINOISE. In this program, a rotor model was tested in the open section wind tunnel DNW, with the purpose of creating an acoustic and aerodynamic database. The measurements were performed at a low Mach number (wind tunnel speed  $\leq 80$  m/s  $\Rightarrow M \leq 0.24$ ), with a traversal microphone array that could travel along the wind tunnel (figure 6). The typical rotor velocity was 1040 RPM. Since the rotor reference frame  $Oxyz$  is rotated of an angle  $\alpha_r$ , relatively to the wind tunnel reference frame  $OXYZ$  (where the microphone coordinates are given), it is necessary to calculate the new microphone coordinates

$$\begin{cases} X = X_{mic} \cos \alpha - Z_{mic} \sin \alpha \\ Y = Y_{mic} \\ Z = X_{mic} \sin \alpha + Z_{mic} \cos \alpha \end{cases} \quad (25)$$

The microphone height was constant for all measurements:  $Z_{mic} = -2.30$  m; the microphones are numbered from 1 to 11, along the  $Y$  axis (table 1).

Table 1: Microphone Positions.

Mic.	1	2	3	4	5	6	7	8	9	10	11
$Y_{mic}$ [m]	-2.70	-2.16	-1.62	-1.08	-0.54	0.00	0.54	1.08	1.62	2.16	2.70

On the table 2, one can find: the microphone  $X_{mic}$  coordinate, the speed of sound in the wind tunnel; the air density  $\rho$ ; the mean flow velocity  $U$ ; the rotor rotation speed  $\omega$ ; the rotor angle of attack  $\alpha_r$ ; the flight path angle (positive for descent)  $\theta_{FP}$ .

The arbitrated parameters are given in table 3. On the second column the pitch angle  $\alpha_p$  is shown; the product of the vorticity and the vortex volume  $|\vec{\Omega}| \vartheta$  is given in column three.

The pitch angle was defined to assure that the blades would have a positive angle of attack. Values were given to the product  $|\vec{\Omega}| \vartheta$ , to present the numerical data with the range given by the experimental data.

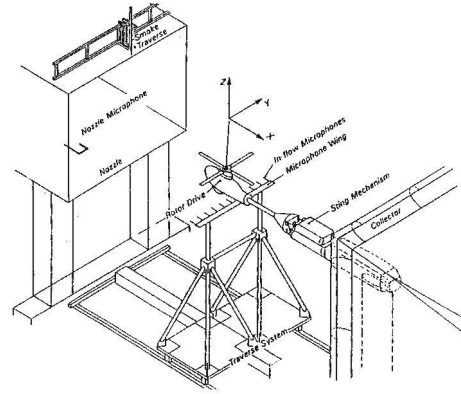


Figure 6: Microphone array, in the DNW wind tunnel.

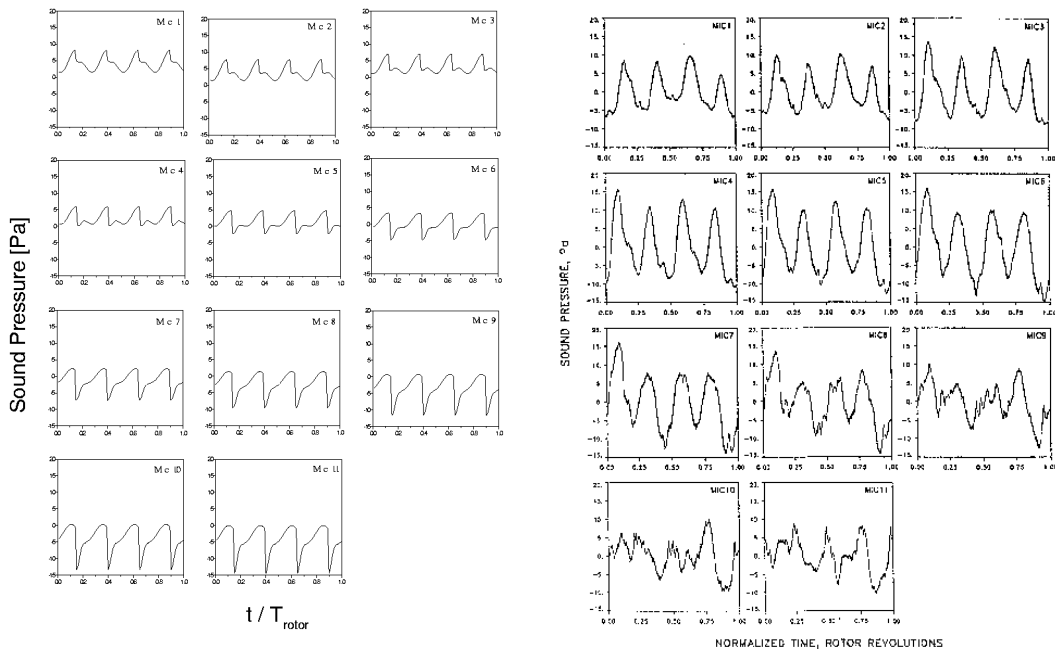


Figure 6: Case I.

Table 2: Cases studied.

Case	$X_{mic}$ [m]	$C$ [m/s]	$\rho$ [kg/m <sup>3</sup> ]	$U$ [m/s]	$\omega$ [RPM]	$\alpha$ [°]	$\theta_{TP}$ [°]
I	0.00	338.92	1.241	60.15	1042	-7.77	0
II	-4.00						

Two cases are presented in this article: both are an typical example of an helicopter travelling at constant altitude (negative angle of attack). The sound pressure numerical data (21) for the normalised rotation time  $T_{rotor}$  and the experimental data, are given in figures 6, 7. As in the experimental data, a transversal translation was simulated and a sound pressure graphic for each microphone is presented.

Table 3: Arbitrated Parameters.

Case	$\alpha_p$ [°]	$ \bar{\Omega}  \vartheta$ [m <sup>3</sup> /s]
I / II	10	1.4

In figure 6, case I is presented. Four pressure peaks are observed, corresponding to the passage of the four blades. Their values decrease, when we go from Microphone 1 to Microphone 11, which is in agreement with the numerical data.

When we make the same study downstream (figure 7), the value of the pressure lower peaks decrease as the microphone number increases (case II). The comparison of the numerical and experimental data could be improved as this simple preliminary model is more refined.

## 5 Conclusions

An analytical model was developed, to study the interaction between a rotor blade and the vortex, generated by the precedent blade. In this simplified model the airfoil has no thickness, which implies a lesser deformation of flow. Besides this important factor, the vortex trajectory is itself altered by the passage of the blade; this effect was also not accounted for. Given the simplicity of the model and the fact that the sound pressure expression is only valid for far field, the data obtained is in fair agreement with the experimental data.

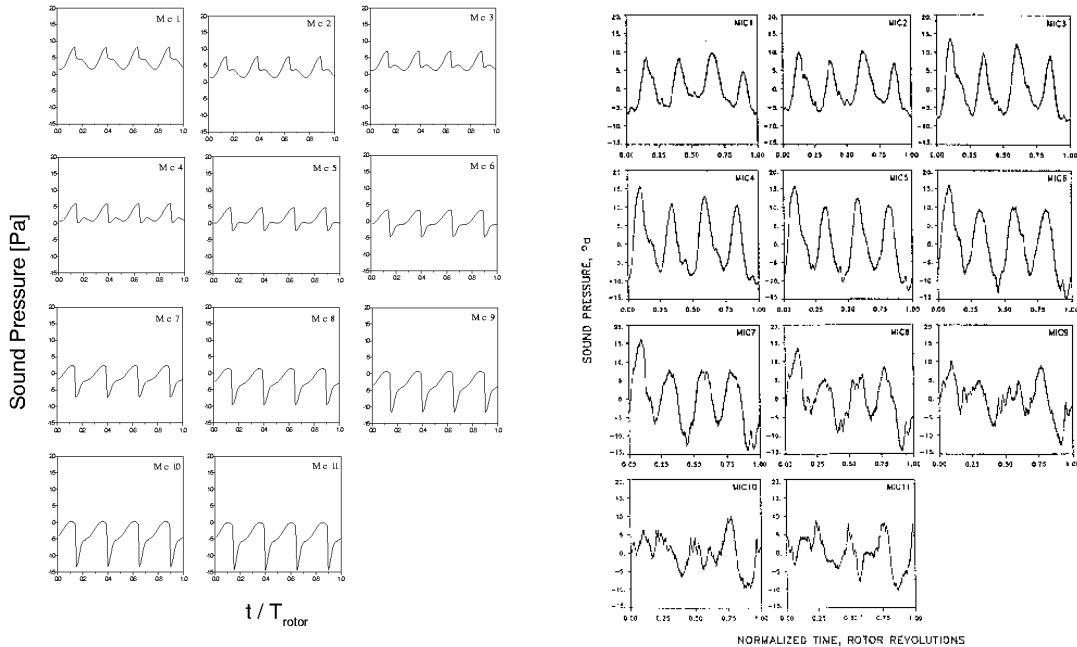


Figure 7: Case II.

## 6 References

- Aravamudan, K.S., Lee, A & Harris, W.L. 1978. A simplified mach number scaling law for helicopter rotor noise, *J. Sound Vib.* **57** (4): 555-570.
- Blokhintsev 1946, D.I. 1946. The propagation of sound in an inhomogeneous and moving medium, *J. Acoustic. Soc. Am.* **18**: 322-344.
- Campos, L.M.B.C. 1978a. On the emission of sound by an ionized inhomogeneity, *Proc. Roy. Soc. London* pp. 65-91.
- Campos, L.M.B.C. 1978b. On the spectral broadening of sound by turbulent shear layers. Part 1: Scattering by interfaces and refraction in turbulence, *J. Fluid. M.* **81**: 529-549.
- Campos, L.M.B.C. 1978c. On the spectral broadening of sound by turbulent shear layers. Part 2: Comparison with experimental and aircraft noise; *J. Fluid M.* **81**: 751-783.
- Campos, L.M.B.C. 1983. Modern trends in research on waves in fluids. Part I: Generation and scattering by turbulent and inhomogeneous flows, *Portugal Phys.* **3-4**: 121-143.
- Campos, L.M.B.C. 1984. On the propagation of sound in nozzles of varying cross-section containing a low mach number mean flow, *Zeitz. Flugwis. Weltrumpf.* **8**: 97-109.
- Campos, L.M.B.C. 1986a On linear and non-linear wave equations for the acoustic of high-speed potential flows, *J. Sound Vib.* **110**: 41-57.
- Campos, L.M.B.C. 1986b. On waves in gases. Part i: Acoustics of jets, turbulence and ducts, *Rev. Mod. Phys.* **58**: 117-182.
- Campos, L.M.B.C. 1988. On generalizations of the doppler factor, local frequency, wave invariant and group velocity, *Wave Motion* **110**: 41-57.
- Campos, L.M.B.C. 1992. On the prediction of the broadband noise of helicopter form the impulsive component, *J. Acoustique* **5**: 531-542.
- Campos, L.M.B.C. & Macedo, C.M. 1992. On the prediction of the broadband noise of helicopter rotors from the impulsive component, *J. Acoustic.* **5**: 531-542.
- Cox, C.R. & Lynn, R.R. 1962. A study of the origin and means of reducing helicopter noise, *Technical report*, U.S. Army Transportation Research Command.
- Dinyavari, M.A.H. & Friedmann, P.P. 1989. Time domain unsteady incompressible cascada airfoil theory for helicopter rotors in hover, *AIAA Journal* **27**: 257-267.
- Farassat, F. 1986. Prediction of advanced propeller noise in the time domain, *AIAA Journal* **24**: 578-584.
- Ffowcs-Williams, J.E. & Hawkings, D.L. 1968. Sound generation by turbulence and surfaces in arbitrary motion, *Phil. Trans. Roy. Soc.* **A264**: 321-342.
- George, A.R. & Lyrintzis, A.S. 1988. Acoustics of transsonic blade-vortex interactions, *AIAA Journal* **26**: 769-776.
- Goldstein, M.E. 1963. *Aeroacoustics*, McGraw-Hill.
- Hawkings, D.L. & Lowson, M.V. 1974. Theory of open supersonic rotor noise, *J. Sound Vib.* **36** (1): 1-20.
- Hawkings, D.L. & Lowson, M.V. Tone noise of high-speed rotors, *Progress in Astronautics and Aeronautics* **44**: 539-558.
- Howe M.S. 1989. On sound generated when a vortex is chopped by a circular airfoil, *J. Sound Vib.* **128**: 487-503.
- Howe, M.S. 1975. Contributions to the theory of aerodynamic sound, with application to excess jet noise and the theory of the flute, *J. Fluid M.* **71**: 625-673.
- Howe, M.S. 1990 Correlation of lift and thickness noise sources in vortex-airfoil interaction, *J. Sound Vib.* **190**: 1-19.
- Humbad, H.G. 1979. Correction to a paper entitled a simplified mach number scaling law for helicopter rotor noise, *J. Sound Vib.* **62** (4): 595-597.
- Landau, L.D. & Lifshitz, E.F. 1953. *Fluid Dynamics*, Claredon.
- Leverton, J.W. & Taylor, F.W. 1966. Helicopter blade slap, *J. Sound Vib.* **4**: 345-357.
- Lighthill, M.J. 1952. On sound generated aerodinamically 1: Turbulence as a source of sound, *Proc. Roy. Soc. London* **A211**: 564-587.
- Lighthill, M.J. 1978. *Waves in Fluids*, Cambridge University Press.
- Lowson, M.V. 1965. The sound field for singularities in motion, *Proc. Roy. Soc. London* **286**: 559-572.
- Lowson, M.V. 1991. Progress towards quieter civil helicopters, *Aeronautical J.* pp. 209-223.
- Morse, P.M. & Ingard, K.U. 1968. *Theoretical Acoustics*, McGraw-Hill.
- Lowson, M.V. & Ollerhead, J. B. 1969. A theoretical study of helicopter rotor noise, *J. Sound Vib.*
- Pierce, A.D. 1981. *Acoustics*, McGraw-Hill.
- Powell, A. 1968. Vortex sound, *J. Acoust. Soc. Am.* **36**: 117-185.
- Rayleigh, J. W. S. 1945. *Theory of Sound*, Dover.
- Röttgermann, A & Wagner, S. 1994. Cost-effective calculation of compressible potential flow around an helicopter rotor including free vortex sheet be a panel method; *AGARD Fluid Dynamics Panel Symp.-*

*Aerodynamics and Aeroacoustics of Rotorcraft, Berlin*, pp. 1-20.

Schmitz, F.H. & Yu, Y.H. 1986. Helicopter impulsive noise: theoretical and experimental status, *J. Sound Vib.* **109** (3): 361-422.

Stangl, R. & Wagner, S. 1994. Euler calculation of the flow field around an helicopter rotor in forward flight, *20th Europ. Rotorcraft Forum*, Amsterdam.

Unal A. & Tung, C. 1989. Two generalized fields and their governing equations applied to helicopter acoustics, *Acustica* **69**: 22-25.

Whitham, G.B. 1974. *Linear and non-linear waves*, Wiley.